



# Surface morphology evolution and underlying defects in homoepitaxial growth of GaAs (110)



Hansung Kim<sup>a,b</sup>, In Won Yeu<sup>c</sup>, Gyuseung Han<sup>c,d</sup>, Gunwu Ju<sup>e</sup>, Yun Joong Lee<sup>b,f</sup>,  
Young-hun Shin<sup>b,g</sup>, Jung-Hae Choi<sup>c</sup>, Hyun Cheol Koo<sup>a,b,\*</sup>, Hyung-jun Kim<sup>b,f,\*</sup>

<sup>a</sup> KU-KIST Graduate School of Converging Science and Technology, Korea University, Seoul 02841, Republic of Korea

<sup>b</sup> Center for Spintronics, Korea Institute of Science and Technology (KIST), Seoul 02792, Republic of Korea

<sup>c</sup> Center for Electronic Materials, Korea Institute of Science and Technology (KIST), Seoul 02792, Republic of Korea

<sup>d</sup> Department of Materials Science and Engineering and Inter-University Semiconductor Research Center, Seoul National University, Seoul 08826, Republic of Korea

<sup>e</sup> Technology Support Center, Korea Institute of Science and Technology (KIST), Seoul 02792, Republic of Korea

<sup>f</sup> Division of Nano & Information Technology, KIST School, Korea University of Science & Technology (UST), Seoul 02792, Republic of Korea

<sup>g</sup> School of Electrical Engineering, Korea University, Seoul 02841, Republic of Korea

## ARTICLE INFO

### Article history:

Received 26 December 2020

Received in revised form 13 March 2021

Accepted 5 April 2021

Available online 10 April 2021

### Keywords:

Gallium arsenide

Crystal growth

Strain

Ab initio calculation

Twinning

## ABSTRACT

The evolution of the surface morphology and underlying pyramidal defects in homoepitaxial GaAs (110) layers was investigated with respect to the layer thickness up to 1  $\mu\text{m}$ . Ga and As atoms coexisting in a one-to-one atomic ratio on the (110)-oriented GaAs surface exhibit different incorporation rates and adatom migration rates, giving rise to local As atomic disordering in the epitaxial layer. Accordingly, this disordering triggers distinctive shapes of three-dimensional surface islands composed of specific facets and underlying microtwins. Single triangular-shaped islands initially appear at an early stage of epitaxial growth. With increasing layer thickness, all of the single triangular islands suddenly become paired triangular islands by forming secondary single triangular islands nearby, like decalcomania. A further increase of the layer thickness induces a complete transformation into four-legged starfish shapes containing directional side edges. At this stage, the underlying pyramidal defects of the surface islands are filled with {111} microtwins. Surprisingly, the evolutions of island shapes and underlying twin formation are closely associated with the strain relaxation in the thick GaAs (110) layers, which is unexpected in any homoepitaxial system. We found that a higher growth temperature retards the shape evolution of surface islands, leading to suppression of compressive strain.

© 2021 The Author(s). Published by Elsevier B.V.  
CC-BY-NC-ND 4.0

## 1. Introduction

Extensive fundamental studies on homoepitaxial GaAs (110) growth have been motivated by interest in fabricating device structures on non-(100)-oriented surfaces and specific applications such as two-dimensional electron gas structures and spintronic devices for longer spin relaxation times [1–5]. However, the fact that homoepitaxial growth of polar III–V compound semiconductors is difficult in the case of (110)-oriented surfaces compared with growth of nonpolar Si and Ge is not widely known; this difficulty stems from the different incorporation rates between group III and group V elements.

Unlike GaAs (100) and (111) surfaces, which consist of alternating Ga and As monolayers stacked perpendicular to the surface, a monolayer of GaAs (110) is composed of equal numbers of Ga and As atoms [6]. Therefore, GaAs (110) itself can be considered a nonpolar surface. However, the differences in the incorporation and surface migration rates between Ga and As adatoms trigger extremely intricate phenomena during further epitaxial growth of III–V compounds, such as unusual surface morphologies resulting from adatom incorporation kinetics and anisotropic adatom migration [6–16]. Consequently, the growth of a high-quality homoepitaxial GaAs (110) layer with a smooth surface morphology should be optimized by controlling growth temperature and the V/III flux ratio within extremely narrow limits.

Joyce et al. extensively studied the surface morphology of GaAs (110) in the early stage epitaxial growth and emphasized the role of the experimental step, which was closely related to the fabrication conditions such as a growth temperature, V/III flux ratio, and As flux

\* Corresponding authors at: Center for Spintronics, Korea Institute of Science and Technology (KIST), Seoul 02792, Republic of Korea.

E-mail addresses: [hckoo@kist.re.kr](mailto:hckoo@kist.re.kr) (H.C. Koo), [mbeqd@kist.re.kr](mailto:mbeqd@kist.re.kr) (H.-j. Kim).

type ( $\text{As}_2$  or  $\text{As}_4$ ) [6–13,15]. According to previous studies, a high V/III flux ratio resulting from the supply of excessive As ( $> 20:1$ ) and a low growth temperature (450–500 °C) are required to obtain a smooth surface without forming three-dimensional (3D) islands [8,11,13]. This condition is presumably ascribed to As exhibiting a lower incorporation coefficient than Ga on the GaAs (110) surface because of preferential thermal desorption of As [14,17]. Triangular islands are a well-known typical 3D characteristic of homoepitaxial GaAs (110) layers and have been intensively investigated on the basis of the surface kinetics of As atom dimerization and adatom migration to clarify their origin [7,8,18,19]. The formation of these islands is apparently suppressed under specific fabrication conditions [8]. However, most previous works have concentrated on suppressing the formation of triangular islands at the early stage of epitaxial growth [7,18,19]. It has been unclear that the underlying defects or strain accumulation triggered by the local nonstoichiometry are closely related to the aforementioned 3D islands. Detailed investigations of the origin of the 3D surface islands, underlying defects, and the corresponding strain are needed to advance the applications of devices based on GaAs (110) with a thickness ranging from a few hundred nanometers to the micrometer scale [20,21].

In this study, we carefully investigated the evolution of the 3D island morphology and underlying pyramidal defects with respect to the thickness of homoepitaxial GaAs (110) layers. In obvious contrast to the previous related works, which mostly examined the triangular surface islands and the consequent surface roughening at low coverages [7,18,19], we found that 3D surface islands evolve through four different stages by changing their shape and dimensions as the GaAs (110) layer thickness is increased to 1  $\mu\text{m}$ . When a GaAs (110) layer reaches the critical thickness, the triangular islands are immediately formed with directional side edges, followed by the formation of paired triangular islands. These paired islands continuously evolve into four-legged starfish-shaped islands and become sharpened. To our knowledge, neither the evolution of the surface island shape nor the corresponding underlying pyramidal defects in homoepitaxial thick GaAs (110) layers has been previously reported. In particular, the starfish-shaped islands have never been observed in the epitaxial crystal growth of any material. Atomic force microscopy (AFM) and X-ray diffraction (XRD) are used to characterize the surface morphology and strain relaxation as functions of the GaAs (110) layer thickness. High-resolution transmission electron microscopy (HRTEM) analyses reveal that two separated underlying pyramidal defects coalesce and become larger at the formation stage of the paired triangular islands. A density functional theory (DFT)-based ab initio thermodynamic method is used to elucidate the stacking fault formation mechanism. The pyramidal defects are found to be agglomerations of entangled stacking faults and multiple microtwins which was occasionally observed in the growth of ZnSe layers [22]. We propose a pathway to suppress the formation of surface islands by reducing the internal compressive strain.

## 2. Experimental

The homoepitaxial GaAs (110) growth experiments were carried out using a molecular beam epitaxy (MBE, Riber Compact 21 T) system. Epi-ready semi-insulating GaAs (110) substrates with an on-axis orientation were pre-baked at 250 °C for 30 min in the introduction chamber of the MBE system. The substrates were immediately transferred to the growth chamber and heated to 610 °C for 10 min under an  $\text{As}_2$  atmosphere to thermally desorb a surface native oxide layer, which was verified by the appearance of ( $1 \times 1$ ) reflection high-energy electron diffraction (RHEED) patterns. The substrate temperature was precisely monitored using a combination of an optical pyrometer and a thermocouple. The homoepitaxial GaAs (110) layers were grown at temperatures ranging from 360°

420°C, which are typical growth temperatures reported in the literature to lead to smooth GaAs (110) surfaces [7,8,11]. The growth rate was fixed at 1.0  $\text{\AA} \text{sec}^{-1}$  with an  $\text{As}_2/\text{Ga}$  incoming flux ratio of 100 to determine the optimum surface morphology. The key experimental variable in this study was the thickness of the GaAs (110) layer, which ranged from 200 to 1000 nm for observation of the evolution of surface islands and underlying pyramidal defects. The surface morphology and island dimensions on the GaAs (110) layers with different thicknesses were examined by AFM of contact mode (Park Systems, XE-100) in air. The crystalline quality and underlying microstructural defects, including stacking faults and multiple twins, were observed using a cross-sectional HRTEM (FEI, Titan 80-300) operated at 300 keV. Furthermore, internal strain stored in the GaAs (110) layers was characterized by XRD in  $\omega$ - $2\theta$  scan mode on a Rigaku ATX-G equipped with a Cu  $K\alpha$  radiation source operated at 12 kW to observe the out-of-plane lattice spacing. The agglomeration of Ga or As atoms at the surface was verified by compositional mapping by electron-probe microanalysis (EPMA, JEOL JXA-8500F) operated at 15 kV.

The DFT calculations were performed using the Vienna Ab initio Simulation Package [23–26]. The projector-augmented wave [27,28] method was used to describe the interaction between core and valence electrons. The local density approximation [29,30] was used as the exchange-correlation functional, with the plane-wave basis function within 500 eV cutoff energy. The 3d, 4s, and 4p electrons of Ga as well as the 4s and 4p electrons of As were treated as valence electrons. The atomic positions were relaxed until the forces were less than  $10^{-4} \text{ eV \AA}^{-1}$  using  $12 \times 12 \times 12$   $k$ -points for the conventional bulk unit cell of zinc-blende-structured GaAs. For the surface-energy calculations, a slab supercell consisting of unreconstructed bottom and reconstructed top surfaces was generated from the relaxed bulk unit cell, where the dangling bonds of the unreconstructed bottom surface were saturated with pseudo-hydrogen ( $Z_{\text{H}} = 1.25$  for a Ga–H bond and  $Z_{\text{H}} = 0.75$  for an As–H bond). When the slab was relaxed, only the atoms in the top five layers were relaxed until the forces were less than  $0.02 \text{ eV \AA}^{-1}$ ; the position of the other atoms at bottom layers, including hydrogen, was fixed. The  $k$ -points along the in-plane directions for the surface slab structures were scaled according to the cell size to maintain a  $k$ -point density similar to that of the bulk unit cell. The convergence of surface energy with respect to the cutoff energy as well as the number of  $k$ -points, atomic layers, and vacuum thickness of the slab was all confirmed, consistent with a previous report [31]. In addition, dipole correction along the vacuum direction was implemented [32].

## 3. Results and discussion

Fig. 1a–e shows 10  $\mu\text{m} \times 10 \mu\text{m}$  AFM height images of GaAs (110) layers grown at 360 °C; the images correspond to different thicknesses of 200, 300, 350, 500, and 1000 nm, respectively. In clear contrast to the absence of characteristic 3D surface features on the 200 nm-thick GaAs (110) layer with a root-mean-square (rms) roughness of 0.573 nm, as shown in Fig. 1a, the thicker GaAs (110) layers in Fig. 1b–e exhibit extraordinary shape evolution of surface islands depending on the layer thickness. Remarkably, the surface islands change shape while maintaining the direction of the side edges. The surface islands have four different specific shapes in Fig. 1: single triangles (b), paired triangles (c), four-legged starfish (d), and sharpened four-legged starfish (e). The single triangular islands have been the most frequently observed feature in previous reports on homoepitaxial GaAs (110) films. Unlike the few-monolayer-high triangular islands reported in previous works [7,18,19], our single triangular islands appear at a thickness of 300 nm and exhibit a much greater average height of 3 nm. The AFM analyses reveal that all of the apexes are exactly oriented along the [001] direction and that the side edges of the single triangular islands are

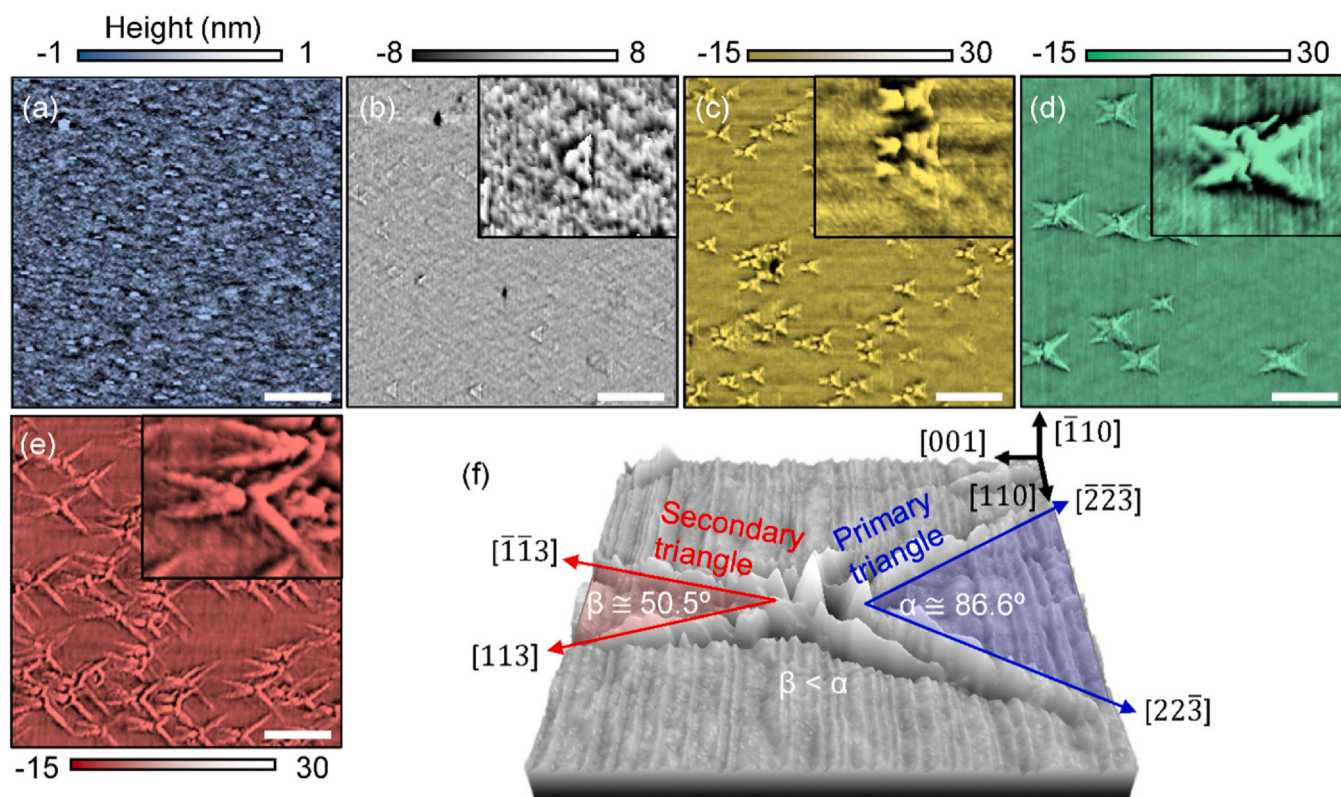


**Fig. 1.** AFM height images of GaAs (110) layers grown at 360 °C to different thicknesses of (a) 200 nm, (b) 300 nm, (c) 350 nm, (d) 500 nm, and (e) 1000 nm. Scale bar is 2  $\mu$ m. The insets in (b)–(e) are the 2.5-fold magnified images of one of the surface islands on the films of different thickness, named (b) a single triangle, (c) a paired triangle, (d) a four-legged starfish, and (e) a sharpened four-legged starfish, respectively. (f) 30°-tilted 3D AFM image of a sharpened four-legged starfish obtained from (e), showing the side edges of primary and secondary triangles with specific directions of  $\langle 113 \rangle$  and  $\langle 223 \rangle$ , respectively.

oriented along the  $[22\bar{3}]$  and  $[\bar{2}\bar{2}3]$  directions. We will later explain that the fixed direction of the side edges is not an accidental event but is related to underlying twins and to the formation of a low-index surface with low energy. The most surprising observation in the 350 nm-thick layer is that all of the individual single triangles become paired triangles by forming a secondary triangle, sharing the apex of a pre-existing primary triangle as shown in Fig. 1c. Whereas the two side edges of the primary triangles maintain the  $\langle 223 \rangle$  direction, those of the secondary triangles have an in-plane direction of  $\langle 113 \rangle$  with a narrower internal angle. Notably, all surface islands on the 350 nm-thick GaAs (110) layer are completely paired triangles. Although numerous authors have reported that the side edges of surface triangles align along either the  $\langle 112 \rangle$  or  $\langle 115 \rangle$  direction [7,11,12,15,18,19,33], the present work is the first observation of paired triangles with two distinctive directions of side edges.

Another important finding is that the body of the triangles subsides by leaving the side edge faceted. This phenomenon begins to occur at a layer thickness of 350 nm and becomes manifest in 500 nm-thick GaAs (110) layers, as shown in Fig. 1c and d, respectively. While both the angles and side-edge directions remain along  $\langle 223 \rangle$  and  $\langle 113 \rangle$ , the lateral dimension of the paired triangles becomes significantly larger as the GaAs (110) layer thickness increases from 350 to 500 nm. In this case, the surface islands are referred to as “four-legged starfish.” Additional epitaxial growth to 1000 nm results in sharpening of the four legs, as displayed in Fig. 1e. At this stage, the leg lengths and internal angles between the primary and secondary triangles are distinguishable, as clearly shown in Fig. 1f, which shows a 30°-tilted 3D AFM image of a sharpened four-legged starfish. That is, the primary triangles possess longer legs and wider internal angles than the secondary triangles.

Although these surface islands are speculated to have originated from structural deformation, they could also have originated from

the compositional agglomeration of Ga atoms, which can occur because of the preferential desorption or disordering of As atoms. The composition of the surface islands was examined by EPMA. Fig. S1 shows 20  $\mu$ m  $\times$  20  $\mu$ m secondary (SL) and backscattered (CP) electron images and the compositional mapping obtained from the same surface area for the four-legged starfish islands formed on a 500 nm-thick GaAs (110) layer. The elemental mapping images reveal that the four-legged starfish are not simple agglomerations of either Ga or As.

Previously reported experimental results obtained from AFM analyses have not explained the relationship between the evolution of the surface island shape and the GaAs (110) layer thickness. We postulate that the evolution is related to the relaxation of strain stored in the thick GaAs (110) layers. Numerous previous studies have examined the homoepitaxial growth of GaAs (110) [7,8,11–13,15,18,19]; however, most of them have focused on single triangular island formation at extremely thin ranges, without considering internal strain and underlying defects. Fig. 2 compares the normal-incidence XRD peaks of the GaAs (110) layers with different thicknesses of 200, 500, and 1000 nm with those of a bare GaAs (110) substrate. This comparison reveals that the most intense peak in all of samples is the GaAs (220) reflection from the substrate. Remarkably, the XRD curves, excluding that of the bare GaAs (110) substrate, show additional peaks that are shifted toward lower angles, indicating that out-of-plane lattice expansion occurred in all of the epitaxial layers because of excess As in GaAs layers grown at low temperature such as 200–300 °C [16,34,35]. The in-plane compressive strain in the three different thicknesses was calculated using the peak shifts relative to the peaks of the substrate considering Poisson ratio and was found to be  $-0.280\%$ ,  $-0.256\%$ , and  $-0.127\%$ , respectively. The decrease in the out-of-plane lattice expansion as the layer thickness is increased to 1000 nm implies a decrease in the in-plane

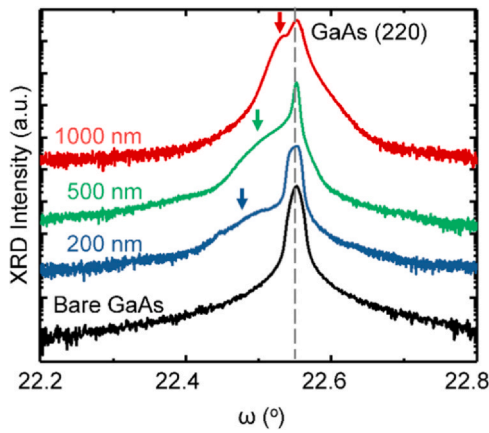


**Fig. 2.** XRD  $\omega$ - $2\theta$  patterns of GaAs (110) layers of three different thicknesses, as compared to the pattern of a bare GaAs (110) substrate. Arrows indicate additional peaks observed at individual thicknesses. The quantitative amount of in-plane compressive strain in the 200, 500, and 1000 nm-thick GaAs (110) layers is  $-0.280\%$ ,  $-0.256\%$ , and  $-0.127\%$ , respectively.

compressive strain, as shown in Fig. 2. We therefore speculate that the formation and evolution of surface islands are closely related to the relaxation of internal strain.

We used TEM to investigate the underlying microstructures of the GaAs (110) layers, which may provide clues about the island shape evolution and the corresponding strain relaxation. Fig. 3 displays a secondary-electron scanning electron microscopy (SE-SEM) image and the corresponding cross-sectional bright-field (BF) TEM image of sharpened four-legged starfish formed on a 1000 nm-thick GaAs (110) layer. For more informative observations, the cross-sectioned sample was cut across the middle of the starfish, as marked in Fig. 3a, to enable simultaneous exploration of the areas underlying the primary and secondary triangles. According to the cross-sectional BF TEM image of the [110] zone axis shown in Fig. 3b, the sharpened four-legged starfish has an underlying pyramidal defect bounded by {111} boundary planes and the inner angle of the lowest

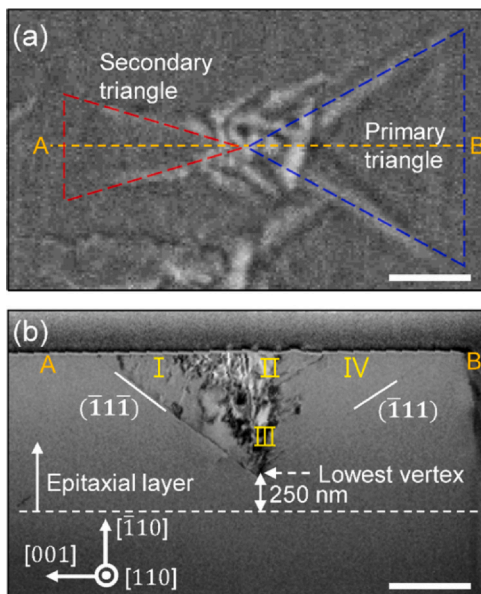


**Fig. 3.** (a) A top-view SE-SEM image of sharpened four-legged starfish formed on 1000 nm-thick GaAs (110) layer; (b) a cross-sectional BF TEM image cut along the dotted line between A and B in Fig. (a). In the pyramidal defect, zones I and IV correspond to the secondary and primary triangles, respectively; zones II and III are the upper and lower parts of the center area below the apex shared by two triangles. Scale bar is 500 nm.

vertex between the  $(\bar{1}11)$  and  $(\bar{1}\bar{1}\bar{1})$  planes is  $109.5^\circ$ . The inside of the underlying pyramid is highly defective compared with the outside, but the defect density is not uniform. In this pyramidal defect, zones I and IV correspond to the region below the secondary and primary triangles, respectively, whereas zones II and III correspond to the upper and lower parts of the center region underneath the apexes, respectively. Zone I appears more defective than zone IV. Zones II and III exhibit the greatest contrast in defects. The two territories of zones I and IV are clearly distinguishable from the defect-free epitaxial layer by the {111} boundary planes. Notably, the lowest vertex of the pyramidal defect is located approximately 750 nm deep in the GaAs (110) epitaxial layer and 250 nm from the substrate surface. Here, the distance of 250 nm between the substrate surface and the lowest vertex of the underlying pyramidal defect is defined as the critical thickness in this study. From this experimental observation, the formation of underlying pyramidal defects and the formation of single primary triangles are reasonably estimated to begin simultaneously at approximately 250 nm thickness. This estimate is further supported by the smooth surface of the 200 nm-thick specimen in Fig. 1a and the appearance of primary triangles on the 300 nm-thick specimen in Fig. 1b.

For a more comprehensive understanding of the formation of pyramidal defects, we thoroughly examined the microstructures using TEM. Fig. 4a–d are BF TEM images showing zones I–IV, respectively, and Fig. 4e–h are HRTEM images of the white-dotted areas in the upper images and the corresponding fast Fourier transform (FFT) diffraction patterns along the  $\langle 110 \rangle$  direction. As predicted by the dark contrast in the center region of the pyramidal defect observed in Fig. 4b and c, zones II and III show a substantially high density of microtwins, as verified by Fig. 4f and g, respectively. This observation is in contrast to that for zones I and IV below the secondary and primary triangles shown in Fig. 4a, d, e, and h. Whereas zone IV has only  $(\bar{1}11)$  twin planes (magnified in Fig. 4h), zone I consists of mostly  $(\bar{1}\bar{1}\bar{1})$  twin planes but  $(\bar{1}\bar{1}\bar{1})$ -s twin planes coexist sparsely (magnified in Fig. 4e). Here, “s” indicates the transformed secondary matrix and is explained in Fig. S3. In addition to the diffraction spots from the zinc blende matrix, conjugate spots from twinning along the  $\langle 111 \rangle$  directions are observed.

The most important finding in the cross-sectional HRTEM observations is that the underlying pyramidal defect is composed predominantly of stacking faults (SFs) and microtwins on {111} planes, which belong to the inherent twin system of GaAs. Because  $\langle 111 \rangle$  is a polar direction, the {111} boundary plane below the primary side can be assigned to either the Ga-terminated (111)A plane, which contains (111),  $(1\bar{1}\bar{1})$ ,  $(\bar{1}\bar{1}\bar{1})$ , and  $(\bar{1}\bar{1}1)$ , or the As-terminated (111)B plane, which contains  $(\bar{1}\bar{1}1)$ ,  $(\bar{1}\bar{1}\bar{1})$ ,  $(1\bar{1}\bar{1})$ , and  $(\bar{1}\bar{1}1)$ . However, both AFM and HRTEM observations show that surface islands and underlying SFs are more easily formed in the primary than in the secondary side, indicating that the plane vulnerable to the SF would be in the primary side. Previous reports estimating the probability of SF formation during epitaxial growth have demonstrated that the crystallographic orientation showing the high-density SF plane corresponds to the one that exhibits a small increase in surface energy as a result of SF formation [36–38].

Therefore, we investigated the preference of SF formation between (111)A and (111)B planes by calculating the surface energy and its increase after SF formation using a DFT-based ab initio thermodynamic method [39]. The surface energy and stable reconstruction of compound semiconductor materials change depending on the growth conditions. Fig. 5a shows the surface energy of GaAs (111)A and (111)B as a function of temperature at a fixed As pressure of  $4 \times 10^{-9}$  atm, which is similar to the MBE growth condition. The vertical dotted line denotes the growth temperature of  $360^\circ\text{C}$ . The most stable reconstruction for each surface is denoted, and the calculated results are in agreement with the in situ RHEED observation that, as temperature increases, the GaAs (111)A surface

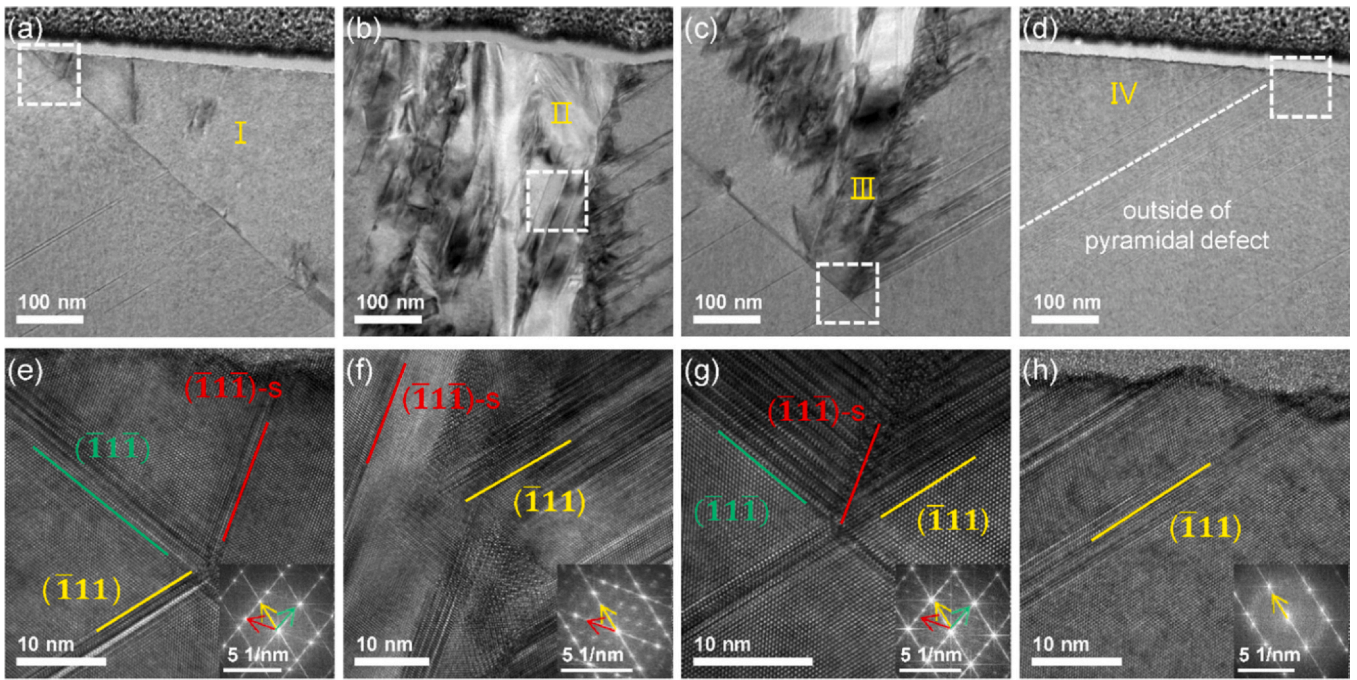


**Fig. 4.** (a)–(d) BF TEM images of zones I, II, III, and IV indicated in Fig. 3; (e)–(h) HRTEM images of the white-dotted areas in (a)–(d). Insets in (e)–(h) show the corresponding fast Fourier transform (FFT) diffraction patterns along the  $\langle 110 \rangle$  direction. Three different twin planes  $-(\bar{1}\bar{1}\bar{1})-s$ ,  $(\bar{1}\bar{1}\bar{1})$ , and  $(\bar{1}\bar{1}\bar{1})-s$  are represented with green, yellow, and red, respectively. Note that the  $(\bar{1}\bar{1}\bar{1})$  twin planes are exactly perpendicular to the  $\langle 111 \rangle$  directions (green, yellow, and red arrows in insets of (e)–(h)).

maintains  $(2 \times 2)$  reconstruction, whereas the  $(111)_B$  surface changes from  $(2 \times 2)$  to  $\sqrt{19} \times \sqrt{19}$  [40]. A Ga-vacancy  $(2 \times 2)$  on the  $(111)_A$  surface and an As-trimer  $(2 \times 2)$  on the  $(111)_B$  surface are the most

stable at  $360^\circ\text{C}$ ; the top views and side views of the corresponding atomic structures are shown in Fig. 5b and c. For these reconstructions, the increase in surface energy resulting from the formation of

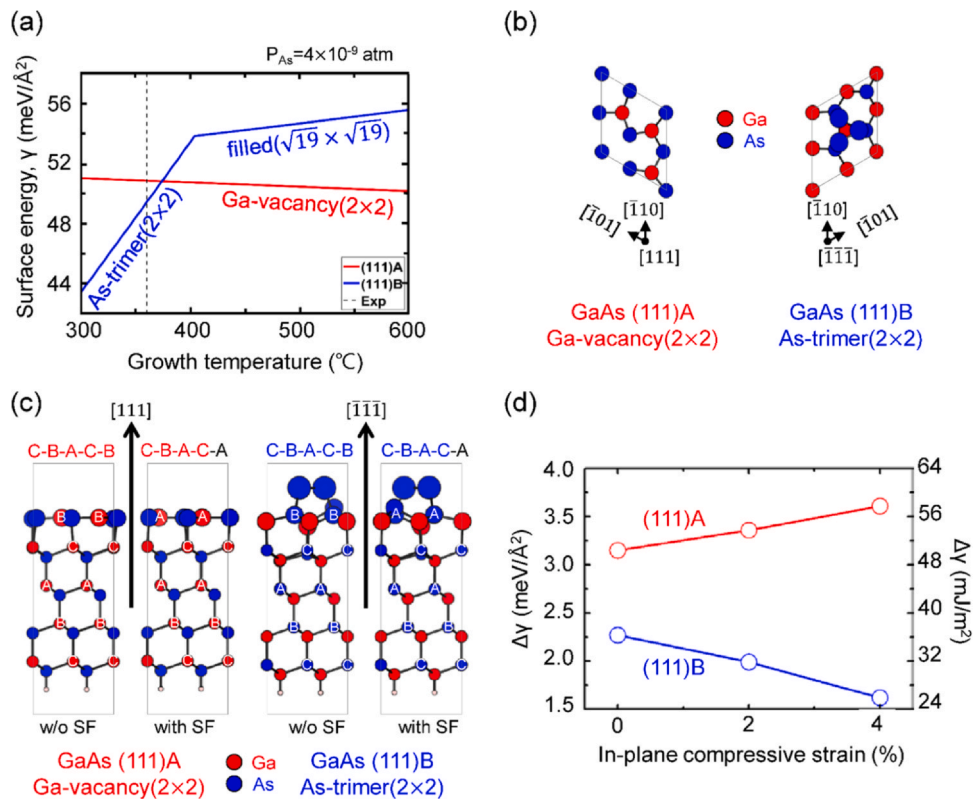


**Fig. 5.** (a) Calculated surface energies ( $\gamma$ ) of GaAs (111)A (red line) and (111)B (blue line); (b) top view of the reconstructed unit cells of the GaAs (111)A Ga-vacancy  $(2 \times 2)$  and (111) B As-trimer  $(2 \times 2)$ . (c) The side view of the GaAs (111)A Ga-vacancy  $(2 \times 2)$  and (111)B As-trimer  $(2 \times 2)$  with and without stacking faults, and (d) the calculated changes in surface energy with increasing in-plane compressive strain. The stacking sequences are denoted from the bottom to the top, as shown above the atomic structures in (c), such that the sequence is C–B–A–C–B for GaAs (111)A Ga-vacancy  $(2 \times 2)$  without a stacking fault. For (c) and (d), the in-plane compressive strain is considered.

SF and its dependence on in-plane strain ( $\epsilon_{xx}$ ,  $\epsilon_{yy}$ ) up to 4% are calculated; the results are shown in Fig. 5d. As the compressive strain increases, the magnitude of the energy increase on the (111)A surface increases from  $3.15 \text{ meV}\text{\AA}^{-2}$  ( $50.4 \text{ mJ m}^{-2}$ ) to  $3.61 \text{ meV}\text{\AA}^{-2}$  ( $57.8 \text{ mJ m}^{-2}$ ); by contrast, that on the (111)B surface decreases from  $2.27 \text{ meV}\text{\AA}^{-2}$  ( $36.3 \text{ mJ m}^{-2}$ ) to  $1.62 \text{ meV}\text{\AA}^{-2}$  ( $25.9 \text{ mJ m}^{-2}$ ). Irrespective of the strain, SF formation is more likely on the (111)B surface than on the (111)A surface and is enhanced by the in-plane compressive strain only on the (111)B surface. This finding explains why the underlying SF and the subsequently formed surface islands are always created on one side (primary, (111)B) and why SF formation, which is one of the strain relaxation mechanisms, is promoted by the accumulated compressive strain, as shown in Fig. 2. After the first SF plane (i.e.,  $(\bar{1}11)$  boundary plane in Fig. 3b) forms above the critical thickness ( $\sim 250 \text{ nm}$  in Fig. 3b), stress is partially released. This release facilitates SF formation on (111)A, which was calculated to be promoted by the relaxation of the in-plane compressive strain. Therefore, the consecutive formation and connecting morphology of the primary and secondary triangles are attributed to the opposite tendency of SF formation with respect to the in-plane compressive strain for the (111)A and (111)B surfaces.

We next investigated the relationship between the surface islands and the underlying pyramidal defects by considering the atomic rearrangement of the SF-induced twin. Fig. S2a and b show a  $30^\circ$ -tilted 3D AFM image of the sharpened four-legged starfish and the corresponding line profile, respectively. To determine the side edges of the sharpened four-legged starfish, two vectors composing the two lines of one side facet on the primary side, named Vector1 (black) and Vector2 (red) in Fig. S2, are denoted as  $[11\bar{x}]$  and  $[\bar{1}1\bar{y}]$ , respectively, where  $x$  and  $y$  are arbitrary positive numbers. Because the (111)B twin plane is located below the primary side of the sharpened four-legged starfish, the atomic arrangement is determined by the twin-transformed coordinates [41]. Fig. S3 shows a schematic of the underlying atomic structures with corresponding transformation matrices and transformed coordinates, where regions rearranged by the (111)A and (111)B twin operations are distinguished by the indices “secondary” (s) and “primary” (p), respectively. Accordingly, the transformed representations of Vector1 and Vector2 are  $\frac{1}{3}[3 - 2x, 3 + 2x, x]$ -p and  $\frac{1}{3}[1 - 2y, -1 + 2y, 4 + y]$ -p, respectively; the cross product of the two vectors,  $\frac{1}{3}[3x + y + 4, 3x - y - 4, 4y - 2]$ -p, is the normal vector of the side facet enclosed by the two vectors. This relationship implies that the possible surface orientations of the side facet vary depending on the combinations of  $x$  and  $y$ . Because of the high surface energy of high-index surfaces, however, only several low-index facets ( $\{100\}$ ,  $\{110\}$ ,  $\{111\}$ A,  $\{111\}$ B) are usually formed in GaAs [42]. If the candidate side facets are constrained to these low-index surfaces, only two combinations are plausible: the  $\{100\}$ -p side facet when  $(x, y) = (1.5, 0.5)$  and the  $\{110\}$ -p side facet when  $(x, y) = (3, 5)$ .

Similar conjecture is applied to the secondary side of the sharpened four-legged starfish by setting Vector3 as  $[11x']$  and Vector4 as  $[\bar{1}1y']$ , as shown in Fig. S2. By transforming to the secondary coordinate system, we obtain the same results as those for the primary side: the  $\{100\}$ -s side facet when  $(x', y') = (1.5, 0.5)$  and the  $\{110\}$ -s side facet when  $(x', y') = (3, 5)$ . In the present study, the side edges on the primary and secondary islands are assigned to  $\langle 223 \rangle$  and  $\langle 113 \rangle$ , respectively, because the angle between the two side edges in a primary island is always larger than that in a secondary island. Notably, the protrusions form specific low-index facets such as  $\{100\}$  and  $\{110\}$  planes by aligning the side edges to the specific direction, which also well matches the observed angle in AFM and SE-SEM images. This alignment is why the surface islands maintain constant directions of side edges irrespective of the GaAs (110) layer thickness and island morphology.

By observing the shape evolution of surface islands along with underlying pyramidal defects composed of several microtwins, we

demonstrated that the shape evolution of surface islands is related to the formation of microtwins to relieve the compressive strain in a homoepitaxial GaAs (110) layer. We verified that the central region in the vicinity of the  $(\bar{1}1\bar{1})$ -s boundary plane in the underlying pyramidal defects is highly defective, as demonstrated in the cross-sectional TEM images in Figs. 3 and 4. However, whether the whole central region consists of high-density microtwins along  $\{111\}$  planes is unclear. The assumption that all of the microtwins from both sides coincide one by one along the  $(\bar{1}1\bar{1})$ -s plane is unreasonable because a time lag occurs between the formation of primary and secondary triangles at the early stage. A series of results clarifies why the microtwins below primary sides form earlier than those below secondary sides. On the basis of the AFM and SEM observations of the sharpened four-legged starfish (Figs. 1e and 3a), the contact point where two apices meet becomes distorted and bumpy with increasing GaAs (110) layer thickness. We speculate that the microtwins of secondary sides coalesce into the preexisting ones of the primary sides at the transition stage from the paired triangle to the four-legged starfish.

Inspired by the literature claiming that excess As is incorporated at low temperatures [16,34,35,43–45], we further increased the growth temperature from  $360^\circ\text{C}$  to  $420^\circ\text{C}$  to fundamentally obstruct the internal strain and suppress the formation of surface islands as well as the underlying microtwins by reducing the concentration of excess As. Fig. 6 shows the surface morphology of 1000 nm-thick GaAs (110) layers grown at increased substrate temperatures of  $400^\circ\text{C}$  and  $420^\circ\text{C}$ . Surprisingly, the formation of the four-legged starfish is greatly suppressed at  $400^\circ\text{C}$  and completely suppressed at  $420^\circ\text{C}$ . This observation indicates that the magnitude of the stored compressive strain becomes lower than that at  $360^\circ\text{C}$ . Meanwhile, another surface feature is observed as a parallel line undulation along the  $[\bar{1}\bar{1}0]$  direction in the layers grown at both growth temperatures. The top surface of the specimen grown at  $420^\circ\text{C}$  shows only parallel line undulation in the absence of any surface islands, resulting in an extremely low rms roughness of  $0.5 \text{ nm}$ , as shown in Fig. 6. The average length of the line undulations of the surface is approximately  $2 \mu\text{m}$ , which is similar to the distance between two ends of primary legs. We speculate that these surface line undulations originate from the microtwins in the outside of the pyramidal defects, as depicted in Fig. 4d.

We already found from XRD analysis that the compressive strain stored in GaAs (110) layers decreases with increasing thickness (Fig. 2). Although the strain is tremendously relaxed at 1000 nm thickness, the residual strain from unwanted surface islands and underlying pyramidal defects remains. Fig. 7 shows the results of the  $\omega$ - $2\theta$  scan mode XRD analysis, which was performed to evaluate the

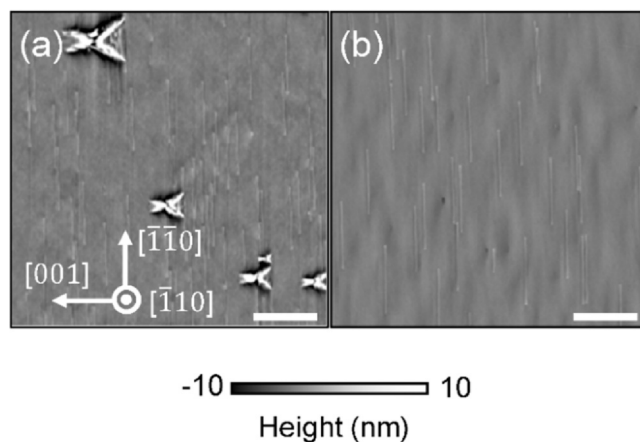
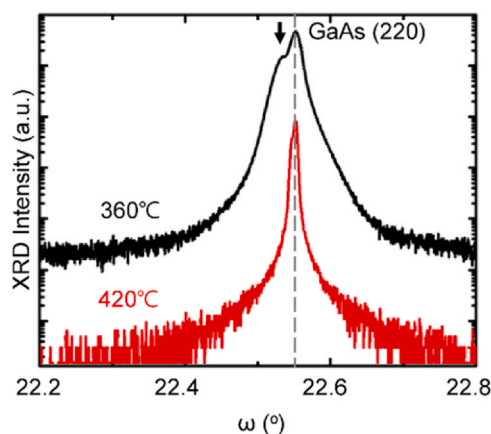


Fig. 6. AFM height images of 1000 nm-thick GaAs (110) grown at (a)  $400^\circ\text{C}$  and (b)  $420^\circ\text{C}$ . Scale bar is  $2 \mu\text{m}$ .



**Fig. 7.** XRD  $\omega$ - $2\theta$  scans of 1000 nm thick GaAs (110) layers grown at different temperatures. An arrow indicates additional peaks resulting from in-plane compressive strain in the GaAs (110) layer grown at 360 °C. No additional peak is observed in the layer grown at 420 °C, indicating no residual internal strain.

internal strain between two growth temperatures of 360 and 420 °C. The GaAs (220) peak in the layer grown at 420 °C becomes sharper without exhibiting peak shift, indicating no internal compressive strain. This experimental result shows that the surface island formation and the subsequent shape evolution are clearly associated with the internal strain induced by excess As.

In this study, we demonstrated the shape evolutions of the surface islands and the corresponding underlying pyramidal defects in the homoepitaxial GaAs (110) layers with respect to their thickness and growth temperature. Our experimental results clearly indicate that the evolutions are strongly associated with the relaxation of compressive strain stored in the layer above the critical thickness. In general, mismatches in lattice constants and thermal expansion coefficients are considered a direct source of internal strain in heteroepitaxial systems. Elastic strain accumulated at the initial stage is eventually released via either cross-hatch dislocations or three-dimensional surface roughening upon the layer reaching the critical thickness. This simple strain-relaxation phenomenon is not directly applicable to homoepitaxial GaAs (110) because of the absence of mismatches in the lattice constants and thermal expansion coefficients. Instead, the strain and relaxation mechanism caused by excess As or local stoichiometric disorder should be carefully studied in terms of polarity and the coexistence of Ga and As atoms on the GaAs (110) surface, which is related to their different incorporation rates. These unusual properties lead to the incorporation of less As into the GaAs (110) layer than into the (100) layer during homoepitaxial growth, which has led some authors to claim that a high As overpressure and low growth temperature are required to achieve a GaAs (110) layer with a two-dimensionally smooth surface [7,11–15,17]. However, further studies on the microstructural analysis of GaAs (110) layers resulting from the greater supply and incorporation of As have not yet been reported. Several studies have focused on the surface morphology and growth mode at the initial stage of growth, mainly using AFM analyses [11,13,15,18]. This approach is in clear contrast to our experimental approach of exploring the shape evolution of the surface islands and microtwins related to strain relaxation at practical thickness ranges. However, the single triangular islands reported in the literature almost certainly result from local stoichiometric disorder such as As dimerization along the side-edge directions irrespective of strain relaxation [7,11,18]. This fact implies that controlling the amount of As incorporated into the GaAs (110) layer to achieve perfect one-to-one Ga/As stoichiometry and crystallinity is difficult. Therefore, the experimental results

obtained in the present study provide useful information about the strain relaxation mechanism of homoepitaxial GaAs (110) layers via formation of surface islands and underlying pyramidal defects. The shape evolution of the surface islands from single triangles to sharpened four-legged starfish and the corresponding pyramidal defect behavior, including the microtwin distributions, are systematically demonstrated with respect to the GaAs (110) layer thickness, which has not been previously reported. Although we deduced a method to suppress the surface islands and underlying pyramidal defects in the thickest GaAs (110) layer of 1000 nm, further optimization of the epitaxial growth conditions is necessary to solve the problem of very-low-density microtwins observed outside the pyramidal defects. The cause of the microtwin formation has not been verified in the present study, and they apparently cannot be originally avoided if they nucleate from the interface via local non-stoichiometric points on the GaAs (110) substrate surface.

Attempts to differentiate the single triangular islands on the 300 nm-thick GaAs (110) layer in the present study from those formed during the very initial growth stage, as reported in the literature [7,18,19], may lead to confusion. The origin of the triangular islands with a height of a few monolayers during the initial growth stage remains a topic of debate. First, preferential growth occurs at the sidewalls of triangle edges in the As-limited regime because of the low As flux and high growth temperature [8]. Second, growth-rate anisotropy results in stabilization of the triangular facets on the (110) surface by As atoms at high As flux and low growth temperatures [46]. Third, triangular facets result from different migration pathways and stable arriving sites for Ga and As adatoms because the most stable sites for the incorporation of incoming adatoms are located along the side edges [18]. Fourth, dimerization of As atoms along the side-edge directions creates an effective energy barrier for adatom surface diffusion, which is presumably a direct cause of the triangular-shaped islands, as commonly postulated [13,47,48]. However, many previous studies have reported various side-edge directions such as  $\langle 112 \rangle$ ,  $\langle 113 \rangle$ , and  $\langle 115 \rangle$  on the basis of experimental observations and simple atomic arrangement modeling. All of the aforementioned origins are controversial and provide no clear explanation for the triangular island formation and the corresponding growth conditions such as a substrate temperature and As flux ratio. We speculate that the single triangular islands are formed at the initial stage through one of the aforementioned mechanisms but then play a pivotal role in strain and relaxation with the emergence of the underlying pyramidal defects.

#### 4. Conclusions

We have investigated the shape evolution of surface islands from single triangles to sharpened four-legged starfish formed on relatively thick homoepitaxial GaAs (110) layers. The surface islands whose formation initiated from the excess As or local stoichiometric disorder are associated with the strain and relaxation at the thick layer above the critical thickness with the formation of the underlying pyramidal defects. The high-density microtwins that occur in the pyramidal defects also play an important role in strain relaxation of the compressive strain stored in the thick GaAs (110) layers. The concentration of excess As is reduced by the higher growth temperature of the GaAs (110) layer, resulting in neither surface islands nor underlying pyramidal defects because less strain is accumulated. We suggested the significantly narrow optimal growth condition suppressing stoichiometric disorder and excess amount of As. These analyses can be used to optimize the growth conditions for other As-based III–V compound semiconductors with (110) orientation, which are expected to have similar adatom kinetics during epitaxial growth as the layers grown in our study.

## CRedit authorship contribution statement

**Hansung Kim:** Validation, Formal analysis, Investigation, Writing - original draft. **In Won Yeu:** Methodology, Formal analysis, Software. **Gyuseung Han:** Methodology, Formal analysis, Software. **Gunwu Ju:** Validation, Visualization. **Yun Joong Lee:** Validation. **Young-hun Shin:** Validation. **Jung-Hae Choi:** Methodology, Supervision, Writing - review & editing. **Hyun Cheol Koo:** Supervision, Writing - review & editing. **Hyung-jun Kim:** Conceptualization, Resources, Writing - review & editing, Project administration.

## Declaration of Competing Interest

The authors declare that they have no known competing financial interests or personal relationships that could have appeared to influence the work reported in this paper.

## Acknowledgments

This work was supported by the National Research Foundation of Korea (NRF) funded by the Korean Government (MEST) (No. 2016910562, 2020M3F3A2A01082147, and 2020R1A2C2003931), the KIST and KU-KIST Institutional Programs, and the Institute of Information & Communications Technology Planning & Evaluation (IITP) (No. 2020-0-00459).

## Appendix A. Supporting information

Supplementary data associated with this article can be found in the online version at [doi:10.1016/j.jallcom.2021.159848](https://doi.org/10.1016/j.jallcom.2021.159848).

## References

- S. Schmult, C. Gerl, U. Wurstbauer, C. Mitzkus, W. Wegscheider, Carbon-doped high-mobility two-dimensional hole gases on (110) faced GaAs, *Appl. Phys. Lett.* 86 (2005) 202105.
- Y. Ohno, R. Terauchi, T. Adachi, F. Matsukura, H. Ohno, Spin relaxation in GaAs (110) quantum wells, *Phys. Rev. Lett.* 83 (1999) 4196–4199.
- A. Hernández-Mínguez, K. Biermann, R. Hey, P.V. Santos, Spin transport and spin manipulation in GaAs (110) and (111) quantum wells, *Phys. Status Solidi B* 251 (2014) 1736–1752.
- O.D.D. Couto Jr., F. Iikawa, J. Rudolph, R. Hey, P.V. Santos, Anisotropic spin transport in (110) quantum wells, *Phys. Rev. Lett.* 98 (2007) 036603.
- W. Wegscheider, G. Schedelbeck, R. Neumann, M. Bichler, (110) oriented quantum wells and modulation-doped heterostructures for cleaved edge overgrowth, *Phys. E: Low Dimens. Syst. Nanostruct.* 2 (1998) 131–136.
- D.M. Holmes, J.G. Belk, J.L. Sudijono, J.H. Neave, T.S. Jones, B.A. Joyce, Differences between As<sub>2</sub> and As<sub>4</sub> in the homoepitaxial growth of GaAs (110) by molecular beam epitaxy, *Appl. Phys. Lett.* 67 (1995) 2848–2850.
- D.M. Holmes, E.S. Tok, J.L. Sudijono, T.S. Jones, B.A. Joyce, Surface evolution in GaAs (110) homoepitaxy: from microscopic to macroscopic morphology, *J. Cryst. Growth* 192 (1998) 33–46.
- E.S. Tok, J.H. Neave, M.J. Ashwin, B.A. Joyce, T.S. Jones, Growth of Si-doped GaAs (110) thin films by molecular beam epitaxy; Si site occupation and the role of arsenic, *J. Appl. Phys.* 83 (1998) 4160–4167.
- E.S. Tok, J.H. Neave, F.E. Allegretti, J. Zhang, T.S. Jones, B.A. Joyce, Incorporation kinetics of As<sub>2</sub> and As<sub>4</sub> on GaAs (110), *Surf. Sci.* 371 (1997) 277–288.
- E.S. Tok, T.S. Jones, J.H. Neave, J. Zhang, B.A. Joyce, Is the arsenic incorporation kinetics important when growing GaAs (001), (110) and (111)A films? *Appl. Phys. Lett.* 71 (1997) 3278–3280.
- P. Tejedor, F.E. Allegretti, P. Šmilauer, B.A. Joyce, Temperature-dependent unstable homoepitaxy on vicinal GaAs (110) surfaces, *Surf. Sci.* 407 (1998) 82–89.
- D.M. Holmes, J.G. Belk, J.L. Sudijono, J.H. Neave, T.S. Jones, B.A. Joyce, The nature of island formation in the homoepitaxial growth of GaAs (110), *Surf. Sci.* 341 (1995) 133–141.
- P. Tejedor, P. Šmilauer, C. Roberts, B.A. Joyce, Surface-morphology evolution during unstable homoepitaxial growth of GaAs (110), *Phys. Rev. B* 59 (1999) 2341–2345.
- H.J. Joyce, J. Wong-Leung, Q. Gao, H.H. Tan, C. Jagadish, Phase perfection in zinc blende and wurtzite III-V nanowires using basic growth parameter, *Nano Lett.* 10 (2010) 908–915.
- P. Tejedor, P. Šmilauer, B.A. Joyce, Growth modes in homoepitaxy on vicinal GaAs (110) surfaces, *Surf. Sci.* 424 (1999) L309–L313.
- M. Lagadas, Z. Hatzopoulos, K. Tsagaraki, M. Calamiotou, C. Lioutas, A. Christou, The effect of arsenic overpressure on the structural properties GaAs grown at low temperature, *J. Appl. Phys.* 80 (1996) 4377–4383.
- M.K. Hudait, Y. Zhu, N. Jain, J.L. Hunter, Structural, morphological, and band alignment properties of GaAs/Ge/GaAs heterostructures on (100), (110), and (111)A GaAs substrates, *J. Vac. Sci. Technol. B* 31 (2013) 011206.
- M. Yoshita, H. Akiyama, L.N. Pfeiffer, K.W. West, Surface-morphology evolution during growth-interrupt in situ annealing on GaAs (110) epitaxial layers, *J. Appl. Phys.* 101 (2007) 103541.
- R. Möller, R. Coenen, B. Koslowski, M. Rauscher, Triangular facets on the GaAs (110) surface observed by scanning tunneling microscopy, *Surf. Sci.* 217 (1989) 289–297.
- X.M. Zhang, D.W. Pashley, I. Kamiya, J.H. Neave, B.A. Joyce, The nucleation and growth by molecular beam epitaxy of InAs on GaAs (110) misoriented substrates, *J. Cryst. Growth* 147 (1995) 234–237.
- T. Kato, T. Takeuchi, Y. Inoue, S. Hasegawa, K. Inoue, H. Nakashima, Stacked GaAs multi-quantum wires grown on vicinal GaAs (110) surfaces by molecular beam epitaxy, *Appl. Phys. Lett.* 72 (1998) 465–467.
- S.K. Hong, B.J. Kim, M.D. Kim, G.S. Park, J.H. Lee, H.S. Park, S.Y. Yoon, T.I. Kim, Determination of defect types of ZnSe-based epilayers by etch-pit configurations, *J. Cryst. Growth* 181 (1997) 343–350.
- G. Kresse, J. Hafner, Ab initio molecular dynamics for liquid metals, *Phys. Rev. B* 47 (1993) 558–561.
- G. Kresse, J. Hafner, Ab initio molecular-dynamics simulation of the liquid-metal-amorphous-semiconductor transition in germanium, *Phys. Rev. B* 49 (1994) 14251–14269.
- G. Kresse, J. Furthmüller, Efficiency of ab-initio total energy calculations for metals and semiconductors using a plane-wave basis set, *Comput. Mater. Sci.* 6 (1996) 15–50.
- G. Kresse, J. Furthmüller, Efficient iterative schemes for ab initio total-energy calculations using a plane-wave basis set, *Phys. Rev. B* 54 (1996) 11169–11186.
- P.E. Blöchl, Projector augmented-wave method, *Phys. Rev. B* 50 (1994) 17953–17979.
- G. Kresse, D. Joubert, From ultrasoft pseudopotentials to the projector augmented-wave method, *Phys. Rev. B* 59 (1999) 1758–1775.
- D.M. Ceperley, B.J. Alder, Ground state of the electron gas by a stochastic method, *Phys. Rev. Lett.* 45 (1980) 566–569.
- J.P. Perdew, A. Zunger, Self-interaction correction to density-functional approximations for many-electron systems, *Phys. Rev. B* 23 (1981) 5048–5079.
- I.W. Yeu, G. Han, J. Park, C.S. Hwang, J.-H. Choi, Theoretical understanding of the catalyst-free growth mechanism of GaAs <111> B nanowires, *Appl. Surf. Sci.* 497 (2019) 143740.
- J. Neugebauer, M. Scheffler, Adsorbate-substrate and adsorbate-adsorbate interactions of Na and K adlayers on Al (111), *Phys. Rev. B* 46 (1992) 16067–16080.
- J.M. McCoy, J.P. LaFemina, Structure and stability of steps on the GaAs (110) surface, *Phys. Rev. B* 54 (1996) 14511–14517.
- M. Kaminska, Z. Liliental-Weber, E.R. Weber, T. George, J.B. Kortright, F.W. Smith, B.-Y. Tsauro, A.R. Calawa, Structural properties of As-rich GaAs grown by molecular beam epitaxy at low temperatures, *Appl. Phys. Lett.* 54 (1989) 1881–1883.
- Z. Liliental-Weber, W. Swider, K.M. Yu, J. Kortright, F.W. Smith, A.R. Calawa, Breakdown of crystallinity in low-temperature-grown GaAs layer, *Appl. Phys. Lett.* 58 (1991) 2153–2155.
- F. Glas, J.-C. Harmand, G. Patriarche, Why does wurtzite form in nanowires of III-V zinc blende semiconductors? *Phys. Rev. Lett.* 99 (2007) 146101.
- X. Yuan, P. Caroff, J. Wong-Leung, L. Fu, H.H. Tan, C. Jagadish, Tunable polarity in a III-V nanowire by droplet wetting and surface energy engineering, *Adv. Mater.* 27 (2015) 6096–6103.
- I.W. Yeu, G. Han, C.S. Hwang, J.-H. Choi, An ab initio approach on the asymmetric stacking of GaAs <111> nanowires grown by a vapor-solid method, *Nanoscale* 12 (2020) 17703–17714.
- I.W. Yeu, J. Park, G. Han, C.S. Hwang, J.-H. Choi, Surface reconstruction of InAs (001) depending on the pressure and temperature examined by density functional thermodynamics, *Sci. Rep.* 7 (2017) 10691.
- D.A. Woolf, D.I. Westwood, R.H. Williams, Surface reconstructions of GaAs (111)A and (111)B: A static surface phase study by reflection high-energy electron diffraction, *Appl. Phys. Lett.* 62 (1993) 1370–1372.
- J.W. Jhang, T. Jain, H.K. Lin, C.W. Lan, Possible twinning operations during directional solidification of multicrystalline silicon, *Cryst. Growth Des.* 18 (2018) 2518–2524.
- I.W. Yeu, G. Han, J. Park, C.S. Hwang, J.-H. Choi, Equilibrium crystal shape of GaAs and InAs considering surface vibration and new (111)B reconstruction: ab-initio thermodynamics, *Sci. Rep.* 9 (2019) 1127.
- Z. Liliental-Weber, TEM study of the structure of MBE GaAs layers grown at low temperature, *Mater. Res. Soc. Symp. Proc.* 198 (1990) 371–376.
- S. Ruvimov, Ch. Dicker, J. Washburn, Z. Liliental-Weber, Twin formation in As precipitates in low-temperature GaAs during high-temperature annealing, *Appl. Phys. Lett.* 72 (1998) 226–228.
- Ph. Ebert, P. Quadbeck, K. Urban, B. Henninger, K. Horn, G. Schwarz, J. Neugebauer, M. Scheffler, Identification of surface anion antisite defects in (110) surfaces of III-V semiconductors, *Appl. Phys. Lett.* 79 (2001) 2877–2879.
- Y. Yasuda, S. Koh, K. Ikeda, H. Kawaguchi, Crystal growth of InGaAs/InAlAs quantum wells on InP (110) by MBE, *J. Cryst. Growth* 364 (2013) 95–100.
- R.L. Schwoebel, E.J. Shipsey, Step motion on crystal surfaces, *J. Appl. Phys.* 37 (1966) 3682–3686.
- G. Ehrlich, F.G. Hudda, Atomic view of surface self-diffusion: tungsten on tungsten, *J. Chem. Phys.* 44 (1966) 1039–1049.